AGU PUBLICATIONS

Geophysical Research Letters

RESEARCH LETTER
10.1002/2017GL076184

Special Section:
Cassini's Final Year: Science Highlights and Discoveries

Intense Harmonic Emissions Observed in Saturn's Ionosphere

A. H. Sulaiman[1], W. S. Kurth[1], A. M. Persoon[1], J. D. Menietti[1], W. M. Farrell[2], S.-Y. Ye[1], G. B. Hospodarsky[1], D. A. Gurnett[1], and L. Z. Hadid[3]

[1]Department of Physics and Astronomy, University of Iowa, Iowa City, IA, USA, [2]NASA Goddard Space Flight Center, Greenbelt, MD, USA, [3]Swedish Institute of Space Physics, Uppsala, Sweden

Abstract The Cassini spacecraft's first Grand Finale orbit was carried out in April 2017. This set of 22 orbits had an inclination of 63° with a periapsis grazing Saturn's ionosphere, thus providing unprecedented coverage and proximity to the planet. Cassini's Radio and Plasma Wave Science instrument repeatedly detected intense electrostatic waves and their harmonics near closest approach in the dayside equatorial topside ionosphere. The fundamental modes were found to both scale and trend best with the H^+ plasma or lower hybrid frequencies, depending on the plasma composition considered. The fine-structured harmonics are unlike previous observations, which scale with cyclotron frequencies. We explore their generation mechanism and show strong evidence of their association with whistler mode waves, consistent with theory. The possibility of Cassini's presence in the ionosphere influencing the resonance and harmonics is discussed. Given their link to the lower hybrid frequency, these emissions may offer clues to constraining Saturn's ionospheric properties.

Key Points:
- First detection of peculiar harmonic emissions in Saturn's topside ionosphere
- The fundamental emissions scale and trend best with the lower hybrid frequency
- Likely associated with the interaction of whistler mode/auroral hiss waves and density irregularities in the topside ionosphere

Supporting Information:
- Supporting Information S1
- Figure S1

Correspondence to:
A. H. Sulaiman,
ali-sulaiman@uiowa.edu

Citation:
Sulaiman, A. H., Kurth, W. S., Persoon, A. M., Menietti, J. D., Farrell, W. M., Ye, S.-Y., … Hadid, L. Z. (2017). Intense harmonic emissions observed in Saturn's ionosphere. *Geophysical Research Letters*, *44*, 12,049–12,056. https://doi.org/10.1002/2017GL076184

Received 26 OCT 2017
Accepted 22 NOV 2017
Accepted article online 1 DEC 2017
Published online 19 DEC 2017

1. Introduction

In the last months leading up to the end of mission, the Cassini spacecraft undertook its final orbits, providing unprecedented coverage and proximity to Saturn. Among other in situ and remote sensing instruments dedicated to observing this unexplored territory, the Radio and Plasma Wave Science (RPWS) instrument (Gurnett et al., 2004) offered electric field measurements across a broad range of frequencies. This revealed some of the usual emissions, such as the whistler mode and Saturn kilometric radiation, in their most intense forms, as well as some new and unfamiliar emissions, one of which is the topic of this letter. Identification and characterization of local plasma waves at Saturn were first established during the Voyager flybys in 1980 and 1981 (Gurnett et al., 1981; Scarf et al., 1982). A more detailed and comprehensive picture has been built since Cassini's Saturn orbital insertion (SOI) in July 2004. Prior to the Grand Finale orbits, Cassini's closest approach (CA) to Saturn had occurred during SOI with a planetocentric distance of under 1.6 R_s (1 R_s = 60,268 km). The first observations summarized by Gurnett et al. (2005) during SOI shed new light on an electrodynamic interaction between the planet and rings.

The Grand Finale orbits, which began in April 2017, had periods of ~6.5 days with a high inclination of 63° and a periapsis between the inner D ring and cloud tops in the dayside. This offered the first opportunity for in situ sampling of Saturn's topside ionosphere (Wahlund et al., 2017). Figure 1 illustrates Cassini's typical trajectory, which was repeated for the 22 proximal orbits, with CA varying between ~1,500 and 4,000 km above the 1 bar surface. The four outermost periapsides were such that the D ring was directly sampled. The spacecraft began its approach from the northern hemisphere and traveled through latitudes from +60° to −60° in less than 2 h.

The electric field-measuring component of the Cassini RPWS instrument consisted of a set of three nearly orthogonal 10 m electric antennas. For the purpose of this study, signals from three of the five onboard receivers are analyzed. Providing continuous low-rate dynamic spectra were the high-frequency receiver (HFR; 3.5 kHz to 16 MHz) and medium-frequency receiver (MFR; 24 Hz to 12 kHz) with high-rate data provided by the wideband receiver (WBR; typically up to 10.5 kHz or 75 kHz, depending on the mode). The spectral resolution is typically 13.6 Hz for the former mode and 109 Hz for the latter mode. The temporal resolution is typically 125 ms/spectrum. While the WBR operated intermittently, data were always available near closest approach for all orbits.

The purpose of this letter is to report first observations, detected by the RPWS instrument, of intense and harmonic fine-structured emissions associated with Saturn's ionosphere. These harmonics are present in each

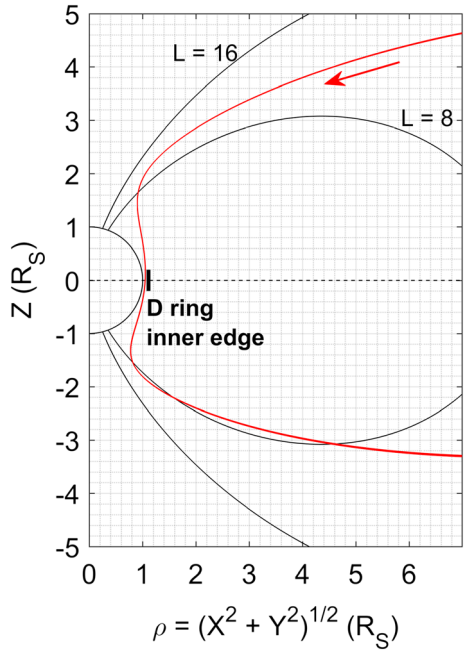

Figure 1. Cassini trajectory (red) during the proximal orbits in the planet-centered planetary solar equatorial orthogonal coordinate system. *X* is defined as positive toward the Sun, *Z* is along the northward spin axis of Saturn, and *Y* is $Z \times X$, completing the right-hand system. The grand finale orbits span Revs 271 to 292. The Cassini spacecraft had a periapsis between the inner edge of the D ring and cloud tops, except for four orbits where the D ring was directly sampled (Revs 276, 277, 281, and 282).

orbit around closest approach. We expand on the nature of these waves by inferring the local plasma properties from dynamic spectrograms of the electric field and comparing the fundamental modes with available characteristic frequencies. These harmonic emissions are, to the best of our knowledge, unlike the commonly observed ion-Bernstein or electrostatic cyclotron harmonic emissions. Finally, we explore the possible generation mechanisms.

2. Observations

Figure 2 shows a low-rate frequency-time spectrogram of the electric field between 21:15 and 23:00 on 29 June 2017 with the relevant ephemeris panel below. The ring plane crossing (labeled RPX) occurred at 22:10 where Cassini sampled the D ring. The presence of dust impacts during RPX is characterized by a burst of intense broadband emissions. From 22:00 to 22:15, the harmonic emissions appeared with the fundamental mode varying between 1 and 10 kHz. More than five additional harmonics are present with similar intensities. These emissions are detected in every orbit of the Grand Finale, though with varying intensities, durations, profiles, and number of visible harmonics.

To explore the nature of these peculiar emissions, we first rule out instrumental artifacts as the source. The semiorthogonal electric field antennas providing signals to the various receivers are labeled E_u, E_v, and E_w. The pair of E_u and E_v was frequently used as a dipole along the spacecraft's *x* axis, E_x, by electronically taking the difference between their voltages (see Figure 14 in Gurnett et al., 2004, for instrument's geometry with respect to spacecraft). Figure S1 in the supporting information shows waveform data captured by the E_x dipole antenna from two different events when the harmonic emissions appear. Clipping of the signal would result in flat peaks and/or troughs in the waveforms, much like square waves, and this generates high nonlinearity (i.e., harmonics in the frequency domain). This is a type of distortion that occurs when the signal exceeds the voltage threshold, thus limiting the output. The waveforms investigated here are fully developed with no evidence of clipping or saturation, thus indicating that these measurements are real.

Now we determine some available plasma properties, most of which can be inferred from the electric field spectra. The electron cyclotron frequency, f_{ce}, in Figure 2 is derived from direct measurements of the magnetic field strength, $|\boldsymbol{B}|$, using Cassini's fluxgate magnetometer (Dougherty et al., 2004), given by f_{ce} (Hz) = 28 $|\boldsymbol{B}|$ (nT). This represents the strongest magnetic field regime Cassini has recorded at Saturn, with a peak f_{ce} of ~500 kHz compared to that during SOI of 300 kHz (Gurnett et al., 2005). Next, we can obtain a handle on the electron number density, n_e, from the whistler mode emissions. The broad (light blue) region centered near RPX is interpreted as a whistler mode emission. This is the only mode that can propagate at these frequencies and typically has a clearly defined upper cutoff boundary. This electromagnetic mode has an upper frequency cutoff at the electron cyclotron frequency or electron plasma frequency, f_{pe}, whichever is lower. Since the emissions' cutoff boundary is well and clearly below the f_{ce} line, this cutoff is set to f_{pe} from which the electron number density can be derived as f_{pe} (Hz) = 8,980 $\sqrt{n_e}$ (cm^{-3}). Deriving the f_Z frequency, a lower cutoff for *Z* mode emissions where $f_Z = \frac{1}{2}(-f_{ce} + \sqrt{(f_{ce}^2 + 4f_{pe}^2)})$, serves as an independent test that verifies this method. Overlaying the f_Z boundary on the spectrograms corresponds extremely well with the *Z* mode (typically narrowband 5 kHz emissions) cessation boundaries (Menietti et al., 2009; Ye et al., 2010), as will be shown in the next section.

3. Discussion

The emissions were inspected for magnetic signatures using the search coil component in the MFR frequency range where this is available. No corresponding signatures were found above the instrument background thus confirming their quasi-electrostatic nature (Stix, 1992). The fundamental emission from Figure 2 is

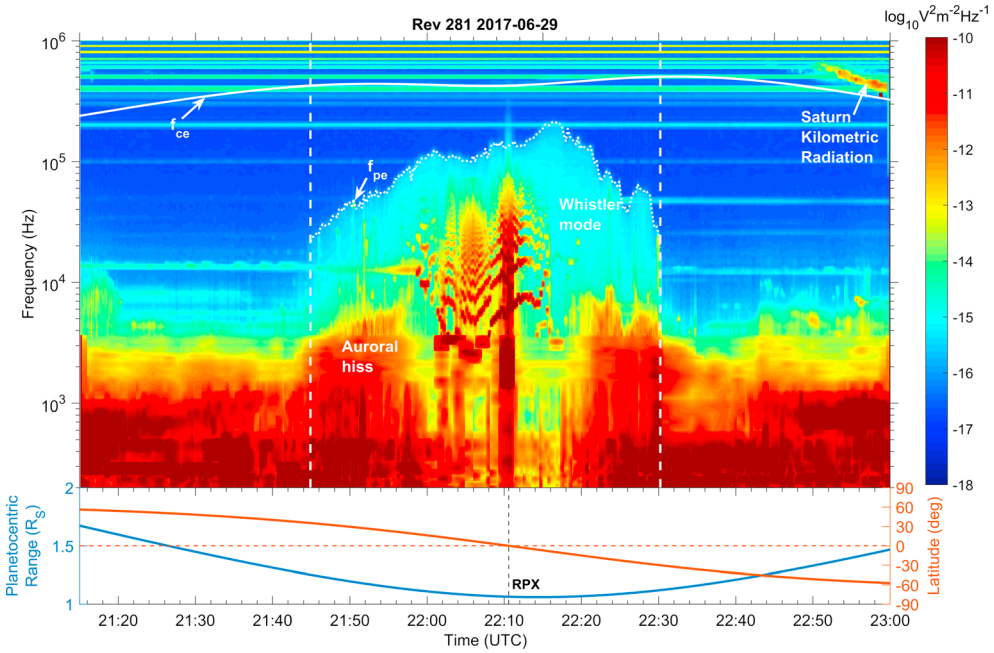

Figure 2. Electric field dynamic spectrogram from the MFR and HFR receivers taken on 29 June 2017. The electron cyclotron frequency is measured directly from the fluxgate magnetometer and represented by the while solid line. The electron plasma frequency is set to the whistler mode cutoff and represented by the dotted line. The dashed lines delimit time history shown in Figure 3, inside which the harmonic fine-banded structures appear. Ephemeris data are plotted in the panel below with the ring plane crossing denoted as RPX.

digitized and compared with characteristic frequencies of the local plasma in the region, as shown in Figure 3. The digitized fundamental emission is represented as a black solid line with the characteristic frequencies as dotted lines. The equatorial plasma here is strongly magnetized, i.e., $f_{ce} \gg f_{pe}$, which represents a parameter space different from previous Cassini orbits where the reverse was true owing to the weaker magnetic field and high electron density from the Enceladus plasma torus. Here the upper hybrid frequency, $f_{UH} = \sqrt{(f_{ce}{}^2 + f_{pe}{}^2)}$, is hence approximately f_{ce}. Altogether, these electron-scale frequencies are at least an order of magnitude higher than that of the fundamental fine-banded emission. The ion cyclotron frequencies of H^+ and $H_3{}^+$, f_{cH+} and f_{cH3+}, respectively, are also included and are at least an order of magnitude lower than the emission.

Next we consider the lower hybrid frequency, a characteristic frequency within this range. For a plasma consisting only of H^+ and electrons, the lower hybrid resonance frequency, f_{LH}, such that $f_{cH+} \ll f_{LH} \ll f_{ce}$, is given by

$$\frac{1}{f_{LH}^2} = \frac{1}{f_{pH+}^2} + \frac{1}{f_{ce} f_{cH+}} \tag{1}$$

where f_{pH+} is the H^+ plasma frequency. In the strongly magnetized plasma regime, where these emissions are observed, equation (1) reduces to $f_{LH} \approx f_{pH+}$ (Brice & Smith, 1965). Assuming quasi-neutrality by setting $n_e = n_{H+}$, the H^+ plasma (and thus the lower hybrid) frequency is computed and overlaid in Figure 3. Further, since Saturn's ionosphere comprises more than one ion species, namely, $H_3{}^+$ (Miller et al., 2000) among other heavier ions, the lower hybrid frequency takes a more general form, which can be computed numerically. This is achieved by solving for the corresponding root of the resonance condition $S = 0$, where S is the first element in the cold plasma dielectric tensor of perpendicular propagating waves (Gurnett & Bhattacharjee, 2017) and is given by

$$S = 1 - \sum_s \frac{f_{ps}^2}{f^2 - f_{cs}^2} \tag{2}$$

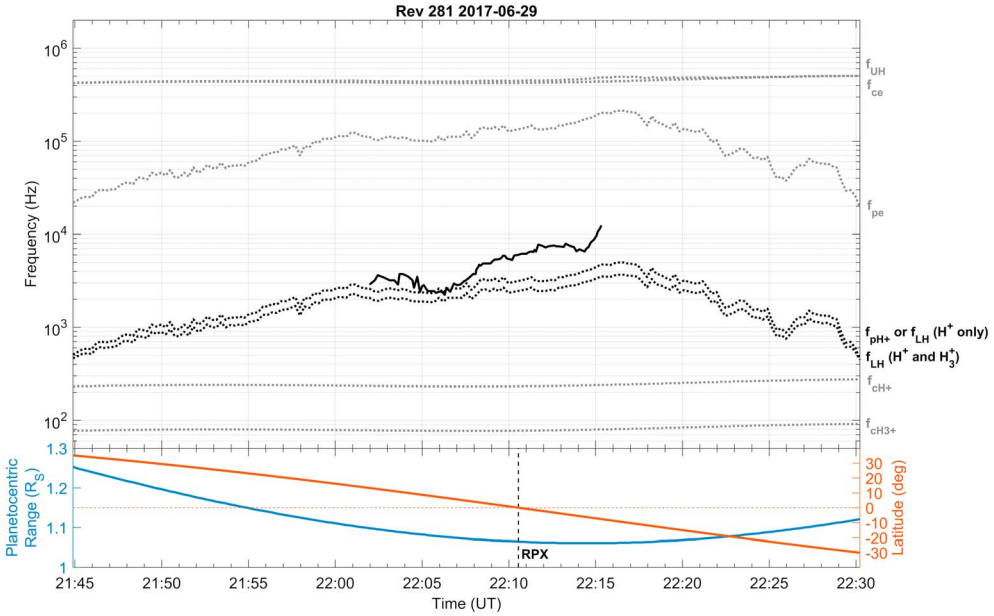

Figure 3. Digitized fundamental mode from Figure 2 (black solid line) plotted in conjunction with the following characteristic frequencies (dotted lines): upper hybrid frequency (f_{UH}), electron cyclotron frequency (f_{ce}), electron plasma frequency (f_{pe}), lower hybrid frequencies (f_{LH}), and H^+ and H_3^+ cyclotron frequencies (f_{cH+} and f_{cH3+}).

with the subscript *s* denoting the species. Solving equation (2) with an additional term for H_3^+ yields a lower hybrid frequency slightly less than that for H^+ alone. Here quasi-neutrality is assumed with equal fractions of H^+ and H_3^+, and this is also overlaid on Figure 3. It is evident that the fundamental emission is scaled best with the lower hybrid frequency in comparison to the other characteristic frequencies, regardless of what ion species or compositions are considered. Note that the maximum possible lower hybrid is that of H^+ only and becomes progressively lower with the addition of more species.

Figure 4 shows segments near CA from two additional orbits: (a) Rev 275 and (b) Rev 279. The electric field spectrograms are from the high-resolution WBR, noting that they are from different modes with frequency ranges of (a) up to 12 kHz and (b) up to 90 kHz. The harmonic emissions are observed in much greater detail near CA, though their profiles differ. The overlaid f_{cH+} lines for both are considerably lower than the fundamental emissions, and conversely, the f_{ce} and f_{pe} lines (not shown) are well above the plotted frequency range. Lower hybrid frequency lines (and their harmonics) assuming H^+ and equal parts of H^+ and H_3^+ show a very good fit to the emissions and their harmonics. More concretely, the lower hybrid frequency lines and the emissions have very similar trends, and this is more obvious at higher harmonics where the variations are augmented. Whereas the emissions are best scaled by the lower hybrid frequency for all orbits, the trending varies between each orbit. Several factors are likely contributors of the offsets between the emissions and lower hybrid lines such as Doppler shift, shortfalls of the quasi-neutrality assumption, species' fractions, and compositions as well as variability (e.g., Kliore et al., 2009).

In this physical picture, since the lower hybrid resonance frequency is much less than the electron cyclotron frequency, the electrons are thus considered to be held motionless by the strong magnetic field. The oscillations are those of the more mobile ions that are free to displace from the fixed negatively charged background. This displacement sets up an electric field that acts as a restoring force driving the oscillations at a characteristic frequency of f_{LH}. For a plasma with only H^+ ions, this characteristic frequency $f_{LH} \approx f_{pH+}$ is reminiscent of electron plasma oscillations except that the ions are mobile rather than the electrons. When other ion species are taken into account, the characteristic frequency becomes some effective ion plasma frequency with relative contributions from other ion populations depending on their masses and proportions.

Lower hybrid resonances are not commonly observed since they require excitation as well as a sufficient condition to be met. Few reports have been made on lower hybrid turbulence at the terrestrial magnetopause

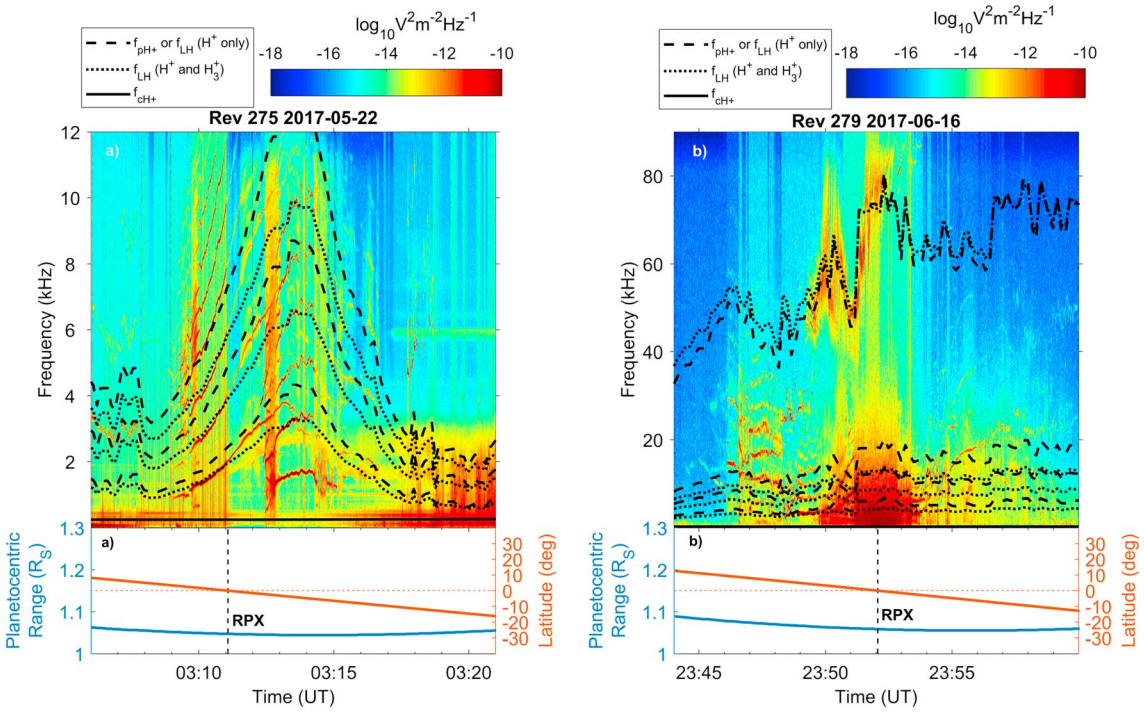

Figure 4. High-resolution dynamic spectra from WBR receiver: (a) 22 May 2017 data from the 10.5 kHz channel and (b) 6 June 2017 data from the 75 kHz channel. Overlaid are characteristic frequencies defined in the text with the first three harmonics of f_{LH} in Figure 4a and the first three and seventeenth harmonic in Figure 4b. For each, two different f_{LH} are derived based on two ion compositions, 100% H^+ and 50% H^+–50% $H_3{}^+$.

(Gary & Eastman, 1979) and the distant magnetotail (Huba et al., 1978). The authors invoke the lower hybrid drift instability driven by density gradients as the source of free energy. Gary and Eastman (1979) and Gurnett et al. (1979) postulate that the excitation is more likely driven by small-scale density and temperature gradients. Cassini detected strong density gradients in the ionosphere, though these are not measurable over ion gyroradii scales owing to the combination of the spacecraft speed and temporal resolution of RPWS. The H^+ gyroradius is on the order of 1 m for a temperature of 0.05 eV (Moore et al., 2008) and a magnetic field strength of 16,000 nT.

The origin of lower hybrid waves is still a subject of debate; however, the consensus among numerous works is that they are associated with interactions of whistler mode waves and density irregularities (Labelle & Treumann, 2002; Lee & Kuo, 1984, and references therein). Bell and Ngo (1990) demonstrated that high-amplitude, short-wavelength electrostatic waves are excited by electromagnetic whistler mode waves. The mechanism is through linear scattering from small-scale field-aligned density gradients, as low as 5%, present in the topside ionosphere. These resulting electrostatic waves cutoff at the lower hybrid resonance frequency and are strongly excited when the scale length of the density irregularity is comparable to the wavelength of the lower hybrid waves, which they found to be 5–100 m. Other works advocate for intense whistler mode auroral hiss as the cause of density irregularities. These then trap the whistler mode waves in eigenmodes and form lower hybrid solitary structures (e.g., Lynch et al., 1996).

Figure 5 represents the best example for evidence of whistler mode emissions associated with lower hybrid waves. Figure 5a shows the low-rate data from Rev 282 with the corresponding high-rate WBR data (up to 10 kHz) in Figure 5b, focusing on the narrowband emissions at 5–7 kHz. Overlaid is the f_Z frequency (derived from the expression in section 2), i.e., the lower cutoff frequency for *Z*-mode waves. The derived f_Z plot matches extremely well with boundaries visible in the narrowband emissions across which the power changes abruptly. Above f_Z (e.g., before 09:15), the narrowband emission is a mixture of *Z* mode and whistler mode. The *Z* mode is ceased at the boundary (e.g., 09:15), after which only the whistler mode propagates until it reaches the region where lower hybrid waves are present. Additionally, funnel-like structure

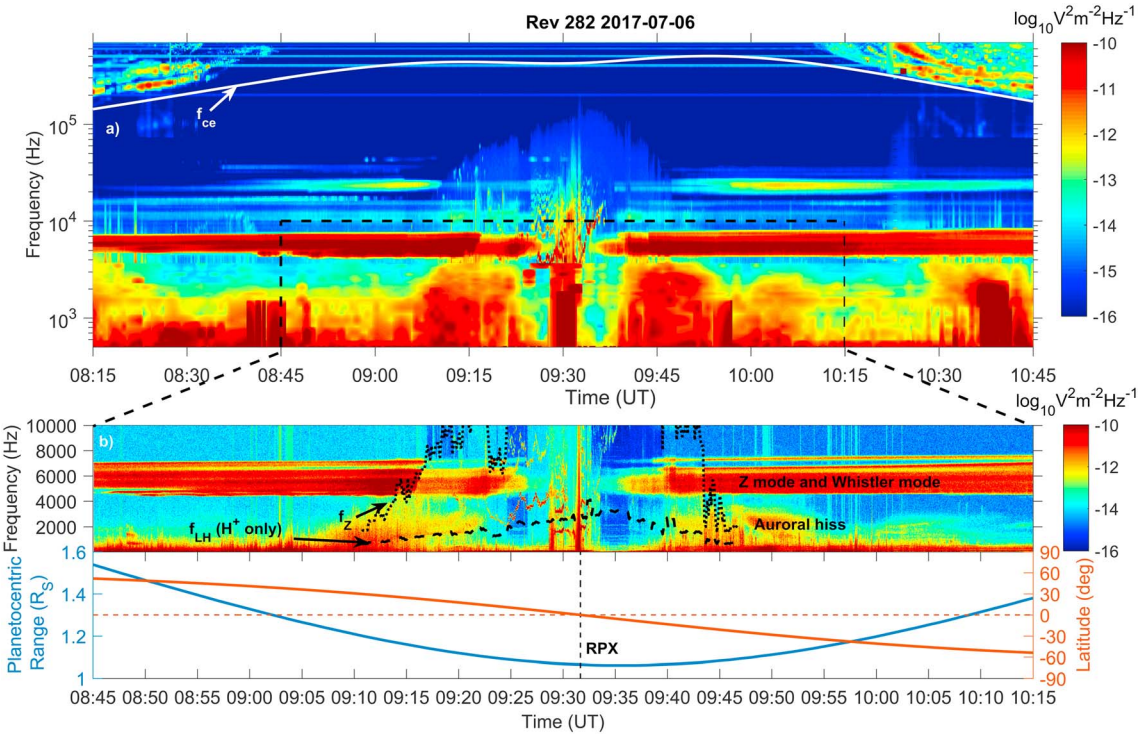

Figure 5. Electric field dynamic spectrograms on 6 July 2017: (a) low-rate HFR and MFR data and (b) high-rate WBR data with the lower hybrid (dashed) and f_Z (dotted) frequencies overlaid.

characteristics of whistler mode auroral hiss are present (e.g., between 09:05 and 09:22) with their lower boundaries lining up extremely well with the overlaid lower hybrid frequency.

While it is not possible to directly confirm the generation mechanisms of the lower hybrid waves put forth by Lee and Kuo (1984), Bell and Ngo (1990), Lynch et al. (1996), and others (Labelle & Treumann, 2002, and references therein), the observations are nevertheless consistent with the consensus among their works to the extent that they are associated with whistler mode waves. There is clear evidence for whistler mode emissions, whether auroral hiss or narrowband, in close proximity to the observations of the lower hybrid emissions. Moreover, their repeated detection in the topside ionosphere, understood to be a prime environment for density irregularities, lends credence to their classification. The source of these density irregularities may be naturally occurring turbulence intrinsic to the ionosphere or generated by the spacecraft's presence. Considering the latter, the parallel wavelength of the lower hybrid emission is on the order of $V_{sc}/f_{LH} \sim 3$ m, where V_{sc} is the spacecraft speed. This is comparable to the spacecraft's dimensions and, by extension, the scale length of the density irregularity that would be caused by its presence.

The harmonic signatures, on the other hand, are atypical of lower hybrid observations. The commonly observed harmonics such as those associated with the ion Bernstein mode are multiples of cyclotron frequencies. In the Grand Finale orbits, there is no evidence of either electron or ion cyclotron harmonics. In contrast, peculiar banded structures associated with the Jovian broadband kilometric radiation have been reported by Cassini RPWS during its Jupiter flyby (Kurth et al., 2001). These were suggested to be a result of electron cyclotron harmonics associated with interchange instability of a density bubble from the outer Io torus (Farrell et al., 2004). Unlike those at Jupiter, the emissions reported here are clearly neither in the electron scale nor were they observed in a similar environment. Harmonic signals are typically associated with highly nonlinear processes at work. We suggest that the probable cause of this nonlinearity is the emissions being affected by the presence of the spacecraft itself given the comparable length scales. We might expect the spacecraft to not only be responsible for triggering the waves but also act as a reflection surface creating multiple sources and consequently altering the wave phasing. This would be analogous to standing waves generating harmonics, much like a string between nodes.

4. Summary and Conclusion

We have presented observations of plasma waves that are manifested as intense and highly harmonic fine-structured emissions in the electric field spectrogram. These have only been observed in Cassini's Grand Finale orbits when the spacecraft grazed Saturn's topside ionosphere. For each orbit, these emissions scaled best with the lower hybrid frequency, which was approximately the H^+ plasma frequency in the regime of a strongly magnetized plasma. Since the lower hybrid is the only resonance in the frequency range between the ion and electron cyclotron frequencies, we thus conclude that these emissions are indeed lower hybrid resonances in the fundamental mode. Their electrostatic nature suggests that they are localized and, by extension, likely to be associated with the ambient ionospheric plasma. It is highly likely that they are associated with whistler mode waves propagating in the ionosphere as postulated by the aforementioned theoretical works (e.g., Bell & Ngo, 1990) and probably generated within small-scale density irregularities owing to the spacecraft's presence. Observations of lower hybrid waves are relatively uncommon in space and planetary environments; hence, much of our understanding of their occurrence and generation comes from theoretical frameworks. In the context of Saturn, their observations make them useful as a proxy for ionospheric composition, particularly with limited particle data set and pointing constraints of the Cassini spacecraft. Further, their detection may offer clues of the extent of density gradients and irregularities in Saturn's ionosphere. For example, the scale of the density irregularities could be estimated from detailed and careful analysis of the associated plasma wave frequencies. Their sources, however, whether detectably influenced by Cassini or intrinsic to the ionosphere such as turbulence, are open to interpretation. The harmonics, on the other hand, remain elusive as they are unlike commonly observed cyclotron frequency harmonics. In a broader context, the study of lower hybrid resonances is of interest to laboratory plasmas. Controlled fusion of tokamak-type plasmas, for example, requires preferential heating of ions, and lower hybrid resonances are thus suggested to be a favorable mechanism to achieve this (e.g., Karney, 1978).

Acknowledgments
The lead author thanks D.L. Kirchner for useful discussions. Cassini RPWS data will be publicly available via NASA's Planetary Data System on a Project-agreed schedule. Prior to this, the data may be requested from the lead author. We acknowledge use of the magnetic field magnitude from the Cassini magnetometer as well as the support of Principal Investigator M.K. Dougherty and data processing/distribution staff. Cassini MAG data were pending recalibration at the time of this study. The research at the University of Iowa was supported by NASA through contract 1415150 with the Jet Propulsion Laboratory.

References

Bell, T. F., & Ngo, H. D. (1990). Electrostatic lower hybrid waves excited by electromagnetic whistler mode waves scattering from planar magnetic-field-aligned plasma density irregularities. *Journal of Geophsysical Research*, *95*(A1), 149–172. https://doi.org/10.1029/JA095iA01p00149

Brice, N. M., & Smith, R. L. (1965). Lower hybrid resonance emissions. *Journal of Geophsysical Research*, *70*(1), 71–80. https://doi.org/10.1029/JZ070i001p00071

Dougherty, M. K., Kellock, S., Southwood, D. J., Balogh, A., Smith, E. J., Tsurutani, B. T., … Cowley, S. W. H. (2004). The Cassini magnetic field investigation. *Space Science Reviews*, *114*(1-4), 331–383. https://doi.org/10.1007/s11214-004-1432-2

Farrell, W. M., Kaiser, M. L., Kurth, W. S., Desch, M. D., Gurnett, D. A., Hospadarsky, G. B., & MacDowall, R. J. (2004). Remote sensing of possible plasma density bubbles in the inner Jovian dayside magnetosphere. *Journal of Geophsysical Research*, *109*. https://doi.org/10.1029/2003JA010130

Gary, S. P., & Eastman, T. E. (1979). The lower hybrid drift instability at the magnetopause. *Journal of Geophsysical Research*, *84*(A12), 7378–7381. https://doi.org/10.1029/JA084iA12p07378

Gurnett, D. A., Anderson, R. R., Tsurutani, B. T., Smith, E. J., Paschmann, G., Haerendel, G., … Russell, C. T. (1979). Plasma wave turbulence at the magnetopause: Observations from ISEE 1 and 2. *Journal of Geophysical Research*, *84*, 7043–7058. https://doi.org/10.1029/JA084iA12p07043

Gurnett, D. A., & Bhattacharjee, A. (2017). *Introduction to Plasma Physics: With Space, Laboratory and Astrophysical Applications*. Cambridge: Cambridge University Press. https://doi.org/10.1017/9781139226059

Gurnett, D. A., Kurth, W. S., & Scarf, F. L. (1981). Plasma waves near Saturn – Initial results from Voyager 1. *Science*, *212*(4491), 235–239. https://doi.org/10.1126/science.212.4491.235

Gurnett, D. A., Kurth, W. S., Kirchner, D. L., Hospodarsky, G. B., Averkamp, T. F., Zarka, P., … Pedersen, A. (2004). The Cassini radio and plasma wave investigation. *Space Science Reviews*, *114*(1-4), 395–463. https://doi.org/10.1007/s11214-004-1434-0

Gurnett, D. A., Kurth, W. S., Hospodarsky, G. B., Persoon, A. M., Averkamp, T. F., Cecconi, B., … Pedersen, A. (2005). Radio and plasma wave observations at Saturn from Cassini's approach and first orbit. *Science*, *307*(5713), 1255–1259. https://doi.org/10.1126/science.1105356

Huba, J. D., Gladd, N. T., & Papadopoulos, K. (1978). Lower-hybrid-drift wave turbulence in the distant magnetotail. *Journal of Geophysical Research*, *83*(A11), 5217–5226. https://doi.org/10.1029/JA083iA11p05217

Karney, C. F. F. (1978). Stochastic ion heating by a lower hybrid wave. *Physics of Fluids*, *21*(9), 1584. https://doi.org/10.1063/1.862406

Kliore, A. J., Nagy, A. F., Marouf, E. A., Anabtawi, A., Barbinis, E., Fleischman, D. U., & Kahan, D. S. (2009). Midlatitude and high-latitude electron density profiles in the ionosphere of Saturn obtained by Cassini radio occultation observations. *Journal of Geophysical Research*, *114*, A04315. https://doi.org/10.1029/2008JA013900

Kurth, W. S., Hospodarsky, G. B., Gurnett, D. A., Lecacheux, A., Zarka, P., Desch, M. D., … Farrell, W. M. (2001). High-Resolution Observations of Low-Frequency Jovian Radio Emissions by Cassini. In H. O. Rucker, M. L. Kaiser, & Y. Leblanc (Eds.), *Planetary Radio Emissions V* (pp 15–28). Vienna: Austrian Academy of Sciences Press.

Labelle, J., & Treumann, R. A. (2002). Auroral radio emissions 1. Hisses, roars and bursts. *Space Science Reviews*, *101*(3/4), 295–440. https://doi.org/10.1023/A:1020850022070

Lee, M. C., & Kuo, S. P. (1984). Production of lower hybrid waves and field-aligned plasma density striations by whistlers. *Journal of Geophysical Research*, *89*(A12), 10,873–10,880. https://doi.org/10.1029/JA089iA12p10873

Lynch, K. A., Arnoldy, R. L., Kintner, P. M., & Bonnell, J. (1996). The AMICIST auroral sounding rocket: A comparison of transverse ion acceleration mechanisms. *Geophysical Research Letters*, *23*(23), 3293–3296. https://doi.org/10.1029/96GL02688

Menietti, J. D., Ye, S. Y., Yoon, P. H., Santolik, O., Rymer, A. M., Gurnett, D. A., & Coates, A. J. (2009). Analysis of narrowband emission observed in the Saturn magnetosphere. *Journal of Geophysical Research*, *114*, A06206. https://doi.org/10.1029/2008JA013982

Miller, S., Achilleos, N., Ballester, G. E., Geballe, T. R., Joseph, R. D., Prange, R., … Hunter Waite, J. (2000). The role of H_3^+ in planetary atmospheres. *Philosophical Transactions of the Royal Society A*, *358*(1774), 2485–2502. https://doi.org/10.1098/rsta.2000.0662

Moore, L., Galand, M., Mueller-Wodarg, I., Yelle, R., & Mendillo, M. (2008). Plasma temperatures in Saturn's ionosphere. *Journal of Geophsysical Research*, *113*, A10306. https://doi.org/10.1029/2008JA013373

Scarf, F. L., Gurnett, D. A., Kurth, W. S., & Poynter, R. L. (1982). Voyager 2 plasma wave observations at Saturn. *Science*, *215*(4532), 587–594. https://doi.org/10.1126/science.215.4532.587

Stix, T. H. (1992). *Waves in Plasmas*. New York: American Institute of Physics.

Wahlund, J.-E., Morooka, M. W., Hadid, L. Z., Persoon, A. M., Farrell, W. M., Gurnett, D. A., … Vigren, E. (2017). In situ measurements of Saturn's ionosphere show that it is dynamic and interacts with the rings. *Science*. https://doi.org/10.1126/science.aao4134

Ye, S.-Y., Menietti, J. D., Fischer, G., Wang, Z., Cecconi, B., Gurnett, D. A., & Kurth, W. S. (2010). Z mode waves as the source of Saturn narrowband radio emissions. *Journal of Geophsysical Research*, *115*, A08228. https://doi.org/10.1029/2009JA015167